Copy
RM L50B09

NACA RM L50B09

RESEARCH MEMORANDUM

WING-FLOW MEASUREMENTS OF LONGITUDINAL STABILITY AND CONTROL CHARACTERISTICS OF A SUPERSONIC AIRPLANE CONFIGURATION HAVING A 42.8° SWEPTBACK CIRCULAR-ARC WING WITH ASPECT RATIO 4.0, TAPER RATIO 0.50, AND SWEPTBACK TAIL SURFACES

By Harold L. Crane and James J. Adams

Langley Aeronautical Laboratory
Langley Air Force Base, Va.

NATIONAL ADVISORY COMMITTEE
FOR AERONAUTICS

WASHINGTON

April 3, 1950

NACA RM L50B09

NATIONAL ADVISORY COMMITTEE FOR AERONAUTICS

RESEARCH MEMORANDUM

WING-FLOW MEASUREMENTS OF LONGITUDINAL STABILITY AND CONTROL CHARACTERISTICS OF A SUPERSONIC AIRPLANE CONFIGURATION HAVING A 42.8° SWEPTBACK CIRCULAR-ARC WING WITH ASPECT RATIO 4.0, TAPER RATIO 0.50, AND SWEPTBACK TAIL SURFACES

By Harold L. Crane and James J. Adams

SUMMARY

This paper presents the results of an investigation at transonic speeds by the wing-flow method of the longitudinal stability characteristics of a 42.8° sweptback supersonic airplane configuration. Lift, pitching-moment, and rolling-moment characteristics of the semispan model as well as stabilizer hinge moments and the effective downwash at the tail were measured over a Mach number range from 0.55 to 1.10 at Reynolds numbers of the order of 600,000. The lift, pitching-moment, and downwash characteristics measured in the present investigation are compared with subsonic and supersonic data for the same configuration from other sources.

The variation of the measured parameters with Mach number was gradual. Peak values of the parameters usually occurred near a Mach number of 0.9. Over the test Mach number range the aerodynamic-center position moved approximately 20 percent chord to the rear with increasing Mach number; the variation of pitching moment with angle of attack tended to remain linear over a larger range of angles of attack at a Mach number of 1.0 or above; at any Mach number in the test range the stabilizer effectiveness was at least as great as at low speeds; the effective downwash at the tail decreased approximately 50 percent over the test Mach number range with most of the decrease occurring near a Mach number of 0.9; the trim changes at zero lift due to Mach number effects were small. The effect of simulated half-blunt (thick trailing edge) ailerons at zero deflection on the lift and moment characteristics was not appreciable.

INTRODUCTION

The Langley Aeronautical Laboratory is conducting by the wing-flow method a series of investigations of the longitudinal stability and control characteristics at transonic Mach numbers of several airplane configurations. As part of this program a semispan model of a supersonic airplane configuration has been tested. The principal features of this configuration were a wing with 42.8° sweepback at the leading edge, a 10-percent-thick symmetrical circular-arc section, an aspect ratio of 4.0, a taper ratio of 0.50 and a 40° sweptback horizontal tail having an NACA 65-008 section.

Measurements were made of lift and pitching moment with the horizontal tail on and off, of rolling moment of the semispan model about the root chord line with tail off, and of hinge moments on the all-movable horizontal tail. The ranges of angle of attack and tail incidence covered were -6° to 12° and -7° to 3°, respectively. The Mach number range was from 0.55 to 1.10 at Reynolds numbers from 360,000 to 840,000. In addition to the preceding tests which gave an indication of the longitudinal stability of this configuration, measurements were also made of effective downwash at the horizontal tail and of the effect of simulated half-blunt ailerons on the longitudinal stability.

This paper presents the results of the outlined investigation and compares the wing-flow data with data for the same configuration from other research facilities.

SYMBOLS

All stability parameters presented are based on the wing span and area of the complete (full-span) configuration. The following symbols and coefficients are used in this paper:

L	lift, pounds
M'	pitching moment (about 23 percent $\bar{c}$), foot-pounds
L'	rolling moment (about root chord line), foot-pounds
H	hinge moment (about -9.5 percent $\bar{c}_t$), foot-pounds
C_L	lift coefficient $\left(\frac{L}{qS}\right)$

[redacted]

C_m pitching-moment coefficient $\left(\frac{M'}{qS\bar{c}}\right)$

C_l rolling-moment coefficient $\left(\frac{L'}{qSb}\right)$

C_h hinge-moment coefficient $\left(\frac{H}{qS_t\bar{c}_t}\right)$

$\frac{dC_m}{dC_L}$ rate of change of pitching-moment coefficient about 23 percent of $\bar{c}$ with lift coefficient

C_{L_α} rate of change of lift coefficient with angle of attack, per degree

C_{m_α} rate of change of pitching-moment coefficient with angle of attack, per degree

C_{l_α} rate of change of rolling-moment coefficient with angle of attack, per degree

C_{h_α} rate of change of hinge-moment coefficient with angle of attack, per degree

$C_{m_{i_t}}$ rate of change of pitching-moment coefficient with tail incidence, per degree

ρ mass density of air, slugs per cubic foot

V free-stream velocity, feet per second

q dynamic pressure, pounds per square foot $\left(\frac{1}{2}\rho V^2\right)$

S wing area, square feet

S_t tail area, square feet

$\bar{c}$ mean aerodynamic chord, feet

$\bar{c}_t$ mean aerodynamic chord of tail, feet

b wing span, feet

M	model Mach number
M_A	airplane Mach number
R	Reynolds number
i_t	tail incidence measured from wing chord line (positive trailing edge down), degrees
ϵ	downwash angle, degrees
α	model angle of attack, measured from wing chord line, degrees
$\frac{\partial \epsilon}{\partial \alpha}$	rate of change of downwash angle with angle of attack

APPARATUS

Photographs of the wing-flow model on the test panel are shown as figure 1. Figure 2 presents sketches of the model showing the principal dimensions. The model consisted of a mahogany fuselage and a high-strength duralumin wing and tail assembly. The end plate which acted as a reflection plane to simulate a full-span condition was 1/50 inch thick. The center-line plane of the model was curved to fit the shape of the test panel so as to conform to the flow along the panel. For one part of the test program, simulated half-blunt ailerons were added to the wing as shown in figure 2(b).

The wing of the model was set at an angle of 3° incidence with respect to the fuselage center line. The wing chord line was used as the reference for measurement of angles of attack and tail settings. The moment reference axis of the test apparatus was located 20 percent of the mean aerodynamic chord ahead of the mean aerodynamic chord, and the all-movable tail rotated on an axis 9.5 percent of the mean aerodynamic chord ahead of the mean aerodynamic chord.

The model was mounted on the right wing of a fighter airplane. The contour of a portion of the wing had been modified to reduce the velocity gradient across the model and to place the wing compression shock behind the model. Plots of the chordwise and vertical gradient are given in figure 3. A chart was prepared from the pressure-distribution data of the average Mach number of the flow over the model as a function of airplane Mach number and lift coefficient. In the workup of data this chart was used to determine the Mach number at the model which, in turn, was used to determine the dynamic pressure at the model.

[redacted]

The aerodynamic forces were measured with a strain-gage balance and the model angles and tail deflections were measured with slide-wire potentiometers. A recording galvanometer made a continuous record of the angles, deflections, and aerodynamic forces. Airspeed, altitude, lateral and normal accelerations, and free-air temperature were recorded with standard NACA instruments. The model attitude angles were recorded with respect to a fixed line on the test panel and these recorded values varied slightly from the angles with respect to the relative wind. A freely floating vane, which was located 22 inches outboard of the model and was calibrated for the difference in angle of flow between the model location and the vane location, was used to determine the angle of flow with respect to the reference line. The angle of flow plus the attitude angle gave the angle of attack.

During flight the model was oscillated by an electric actuator which varied the angle of attack at a rate of 1 cycle per second. In flights in which the tail was oscillated, an air-driven motor was used to oscillate the tail at the rate of 1 cycle per second. These rates of oscillation resulted in a maximum rate of rotation of approximately 1° per 66 chord lengths of motion with respect to the air stream, which is believed to be sufficiently small to approximate static conditions.

TESTS

The following test runs were made:

(1) Tail off, model oscillating between 12° and -6° (angle of attack and tail incidence are measured with respect to the wing chord line) with and without simulated half-blunt ailerons

(2) Tail on and fixed at 0°, model oscillating between 12° and -6° with and without simulated half-blunt ailerons

(3) Tail on and fixed at -5° (trailing edge up) model oscillating between 12° and -6°

(4) Model fixed at 0°, tail oscillating between 3° and -7°

(5) Model fixed at 5°, tail oscillating between 3° and -7°

(6) Model oscillating, tail free to trim (The effective downwash at the tail was thereby determined.)

During each flight, runs were made at two different altitudes in order to furnish the largest possible range of Reynolds number. A high-dive run was made from an altitude of 28,000 feet to 22,000 feet.

[redacted]

This procedure furnished local Mach numbers over the model of 0.65 to 1.10 and Reynolds numbers from 360,000 to 620,000. A low dive from 18,000 feet to 8,000 feet furnished local Mach numbers of 0.55 to 1.00 and Reynolds numbers from 400,000 to 840,000. A plot of Reynolds number based on the mean aerodynamic chord of the wing against Mach numbers is given in figure 4.

PRESENTATION OF RESULTS

A view of a sample record from the six-element galvanometer is presented in figure 5. Ground records taken with the model oscillating indicate that the irregularities in the pitching-moment trace were introduced by the driving mechanism.

Typical plots of the wing-flow data showing the test points are presented in figure 6 to illustrate the amount of scatter that occurs in the data. Figure 6(a) contains plots of lift coefficient and pitching-moment coefficient against angle of attack for the complete model with the tail set at 0° at a Mach number of 1.0. Figure 6(b) is an example of the data used for determination of effective downwash, a plot of tail incidence with the tail free against angle of attack at $M = 1.0$.

An estimation of the accuracy of the various measurements is presented in the following table:

Variable	Approximate possible error		
	In absolute value	In coefficient	
		At minimum q 200 lb/sq ft	At maximum q 800 lb/sq ft
Mach number, M	±0.02	------	------
Dynamic pressure, q, percent	±2.0	------	------
Angle of attack, α, deg	±0.5	------	------
Tail incidence, i_t, deg	±0.5	------	------
Lift, L, lb	±1.0	±0.06	±0.02
Pitching moment, M, in-lb	±1.0	0.03	0.01
Rolling moment, L', in-lb	±1.0	0.004	0.001
Hinge moment, H, in-lb	±0.1	0.03	0.01

Approximate possible errors in the values of measured quantities and in the coefficients of force and moment are presented. The approximate possible errors in the coefficients tend to vary inversely with dynamic pressure and are presented for the minimum and maximum dynamic pressures. The values of possible errors presented do not take into account the

effects of the velocity gradient over the model. It should be noted that errors in increments of any measured variable determined from the faired curves presented herein will be considerably smaller than errors in absolute values.

The variation of lift and moment coefficients with angle of attack or tail incidence are presented in figure 7 for the tail-off case, in figure 8 for the tail-on configuration with $i_t = 0^\circ$, and in figure 9 for the tail oscillating case with $\alpha = 0^\circ$. The symbols used on these curves are for identification only and do not represent test points. The data are presented for increments of Mach number of 0.05 or 0.10 throughout the test range for the two Reynolds number ranges.

The slopes C_{L_α}, C_{m_α}, and C_{l_α} at an angle of attack of 0° for the tail-off and tail-on configurations are presented as a function of Mach number in figures 10 and 11. Figure 12 shows the slope $C_{m_{i_t}}$ as a function of Mach number for the tail oscillating case.

The variation of tail incidence for zero hinge moment with angle of attack for Mach numbers throughout the test range and for the two Reynolds number ranges are presented in figure 13. Figure 14 gives the variation with Mach number of the effective downwash factor $\frac{\partial \epsilon}{\partial \alpha}$ at the tail which was determined from the data of figure 13.

DISCUSSION OF RESULTS

Tail-Off Characteristics

Throughout the test Mach number range there did not appear to be any large or abrupt change in the lift characteristics for small angles of attack. The decrease in slope of the lift and half-model rolling-moment curves of figure 7 at moderate angles of attack which is more pronounced with the rolling-moment curves indicates that early loss in lift occurred over the outboard portion of the wing. This effect was reduced or postponed to a higher angle of attack for Mach numbers equal to or greater than 1.0. Variation of the angle of zero lift or the lift coefficient at an angle of attack of 0° with Mach number was negligible.

The variation of spanwise center of pressure of the wing-fuselage combination with Mach number and angle of attack was determined from the data of figure 7 by taking ratios of half-span rolling-moment or bending-moment coefficients and lift coefficients. The center of pressure was found to be between 45 and 48 percent of the semispan for small angles of attack over the test Mach number range. The center of pressure moved

inboard roughly 8 percent of the semispan with increasing angle of attack. Above a Mach number of 1.0 the inboard movement of the center of pressure with increasing angle of attack was somewhat reduced. No correction has been made for any effect which the end plate might have on the half-span rolling moments. The end plate could conceivably produce a counter moment equal to a few percent of the wing rolling moment.

The lift-curve slope with tail off obtained from the wing-flow data at a Mach number of 0.55 at an angle of attack of 0° was 0.07 as compared with the value of approximately 0.065 which was obtained by correcting the low-speed lift-curve slope measured from figure 12 of reference 1 for the effects of Mach number. This and other comparisons indicate that the lift-curve slopes obtained in this investigation by the wing-flow method are probably somewhat high. Figure 10 indicates that C_{L_α} increased gradually with Mach number to a peak value of approximately 0.08 at $M = 0.8$. Above a Mach number of 0.8, C_{L_α} decreased gradually to approximately 0.06 at $M = 1.1$. These lift-curve slopes were obtained from the higher Reynolds number data which were extrapolated to a Mach number of 1.1 by reference to the lower Reynolds number data.

The plots of pitching-moment coefficient in figure 7 indicate that for a center-of-gravity position at 23 percent mean aerodynamic chord the test configuration was stable with the horizontal tail removed at low angles of attack. The low-speed tests of reference 2 did not show any such unusual stability condition with the horizontal tail off. For larger angles of attack for which the outboard portion of the wing lost effectiveness, the variation of pitching moment with angle of attack became unstable. At Mach numbers of 1.0 or above the variation of pitching moment with angle of attack remained stable to considerably greater angles of attack. The slope C_{m_α} at an angle of attack of 0°, which is presented in figure 10, tended to become more negative with increasing Mach number. It should be noted that at the lower Mach numbers for which the variation of C_m with α was very nonlinear, the slope measured at 0° has little meaning.

Tail-On Characteristics

Addition of the horizontal tail increased the lift-curve slope approximately 10 percent. The effects of Mach number and tip stalling on the variables were approximately the same as those with the tail off. There was little variation with Mach number of the pitching-moment coefficient at an angle of attack of 0°.

Aerodynamic-center positions of the complete test configuration at small angles of attack were determined from the ratios of the slopes C_{m_α} and C_{L_α} of figure 11(a). The variation of the aerodynamic-center

position with Mach number is presented in figure 11(b). The figure shows that the aerodynamic-center position gradually moved rearward from about 35 percent to approximately 60 percent mean aerodynamic chord as the Mach number increased from 0.55 to 1.1. Low-speed tests of the same configuration at approximately 4 times the Reynolds number indicated that the aerodynamic center at small angles of attack was at approximately 35 percent mean aerodynamic chord. (See reference 2.)

Lift and pitching-moment data for the test configuration were available at a Mach number of 0.16 from reference 2, at a Mach number of 1.40 from reference 3, and at Mach numbers of 1.55, 1.90, and 2.32 from reference 4. Figure 15 shows the data of references 2, 3, and 4 along with wing-flow data in the form of plots of C_L and C_m against α at various constant Mach numbers for a center-of-gravity position of 25 percent mean aerodynamic chord. The figure indicates, approximately, the effect of Mach number on the variation of lift coefficient with angle of attack and on the longitudinal stability of the test configuration. This effect took the form of a gradual variation of the slopes C_{L_α} and C_{m_α} with Mach number, first increasing and then decreasing through the transonic range. Figure 15 also provides a guide for assessing the reliability of the wing-flow data.

Tail Effectiveness

The data of figure 9 indicate that the horizontal tail of the wing-flow model was subject to stalling at a very small angle of attack at the test Reynolds numbers. The absolute value of the tail effectiveness as indicated in figure 12 by the slope $C_{m_{i_t}}$ at $i_t = 0^\circ$ increased with increasing Mach number up to $M = 0.8$ and then decreased gradually up to $M = 1.10$, the maximum test Mach number. It should be kept in mind that the variation of C_m with i_t was nonlinear, especially at the lower Mach numbers.

Downwash

As shown in figure 14 the effective downwash factor $\frac{\partial \epsilon}{\partial \alpha}$ at the horizontal tail was approximately 0.45 at a Mach number of 0.55 and increased to approximately 0.50 at $M = 0.9$. Above a Mach number of 0.9, $\frac{\partial \epsilon}{\partial \alpha}$ decreased steadily to approximately 0.33 at $M = 1.1$. The value of $\frac{\partial \epsilon}{\partial \alpha}$ obtained at $M = 0.55$ agreed closely with a low-speed value from reference 2. Figure 16 is a plot of effective downwash against angle of attack for $M = 0.16$ from reference 2, $M = 0.55$ and 1.10 from the

[redacted]

wing-flow data, and $M = 1.40$ from reference 3. These data indicate that the variation of downwash at the tail with angle of attack is similar at Mach numbers throughout the subsonic and transonic range.

Effect of Half-Blunt Ailerons

Tests were made with half-blunt ailerons attached to the wing, as shown in figure 2(b), in an attempt to measure the effects on lift, pitch, and drag of the half-blunt ailerons at a deflection of 0°. However, any effects that may have been present were small enough to be within the accuracy of the balance and could not be definitely detected.

CONCLUDING REMARKS

The results of an investigation by the wing-flow method of the longitudinal stability characteristics of a 42.8° sweptback supersonic airplane configuration indicated that:

1. The trim changes at zero lift with increasing Mach number were small up to the maximum test Mach number of 1.10.

2. The aerodynamic center of the complete airplane configuration gradually shifted approximately 20 percent mean aerodynamic chord to the rear as the test Mach number increased from 0.55 to 1.10.

3. The stabilizer effectiveness varied gradually with Mach number and was approximately as great at a Mach number of 1.10 as at a Mach number of 0.55.

4. The effective value of the downwash factor $\frac{\partial \epsilon}{\partial \alpha}$ at the tail for small angles of attack was approximately constant at 0.45 below a Mach number of 0.85. Between 0.85 and 0.90, $\frac{\partial \epsilon}{\partial \alpha}$ increased to approximately 0.50 and then decreased to approximately 0.33 at a Mach number of 1.10.

5. The effect of simulated half-blunt ailerons at zero deflection on the lift and moment characteristics was not appreciable.

Langley Aeronautical Laboratory
National Advisory Committee for Aeronautics
Langley Air Force Base, Va.

REFERENCES

1. Neely, Robert H., and Koven, William: Low-Speed Characteristics in Pitch of a 42° Sweptback Wing with Aspect Ratio 3.9 and Circular-Arc Airfoil Sections. NACA RM L7E23, 1947.

2. Weil, Joseph, Comisarow, Paul, and Goodson, Kenneth W.: Longitudinal Stability and Control Characteristics of an Airplane Model Having a 42.8° Sweptback Circular-Arc Wing with Aspect Ratio 4.00, Taper Ratio 0.50, and Sweptback Tail Surfaces. NACA RM L7G28, 1947.

3. Spearman, M. Leroy: An Investigation of a Supersonic Aircraft Configuration Having a Tapered Wing with Circular-Arc Sections and 40° Sweepback. Static Longitudinal Stability and Control Characteristics at a Mach Number of 1.40. NACA RM L9L08, 1950.

4. Ellis, Macon C., Jr., Hasel, Lowell E., and Grigsby, Carl E.: Supersonic-Tunnel Tests of Two Supersonic Airplane Model Configurations. NACA RM L7J15, 1947.

[redacted]

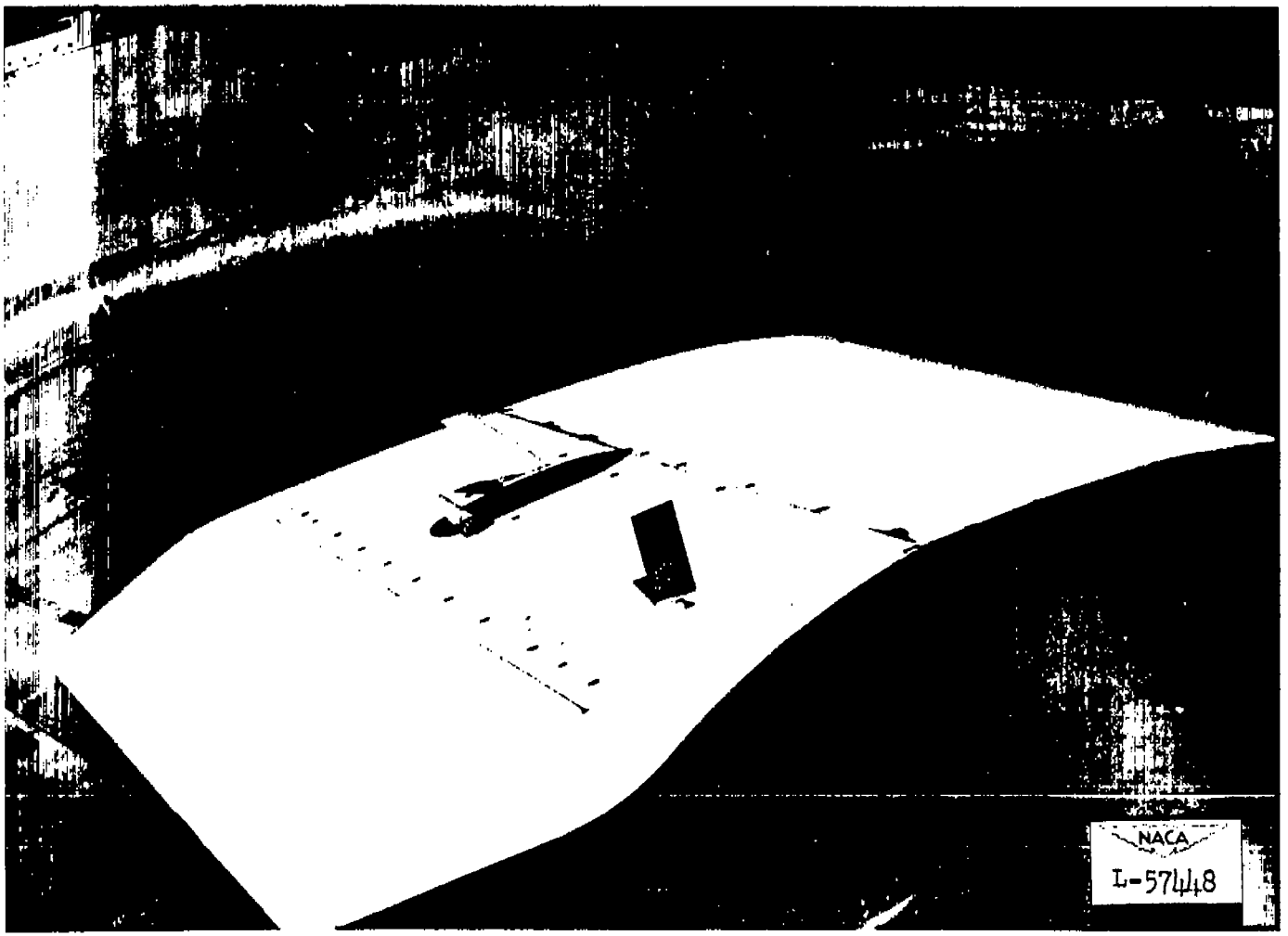

(a) View of model mounted on test panel. Flow angle vane is shown in foreground.

Figure 1.- Photographs of model.

(b) Close-up of model mounted on test panel.

Figure 1.- Concluded.

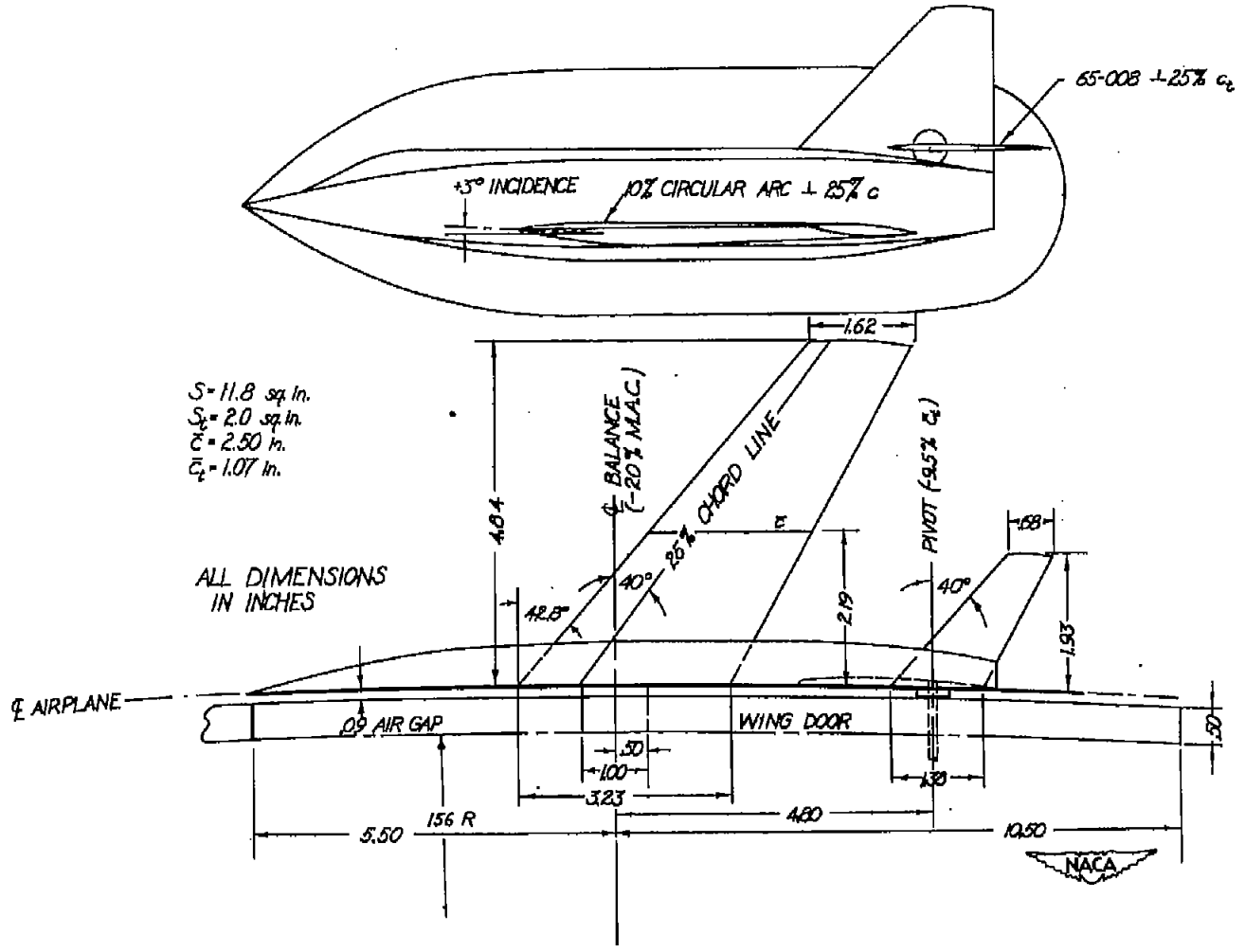

(a) Top and side views of model.

Figure 2.- Drawings of model showing principal dimensions.

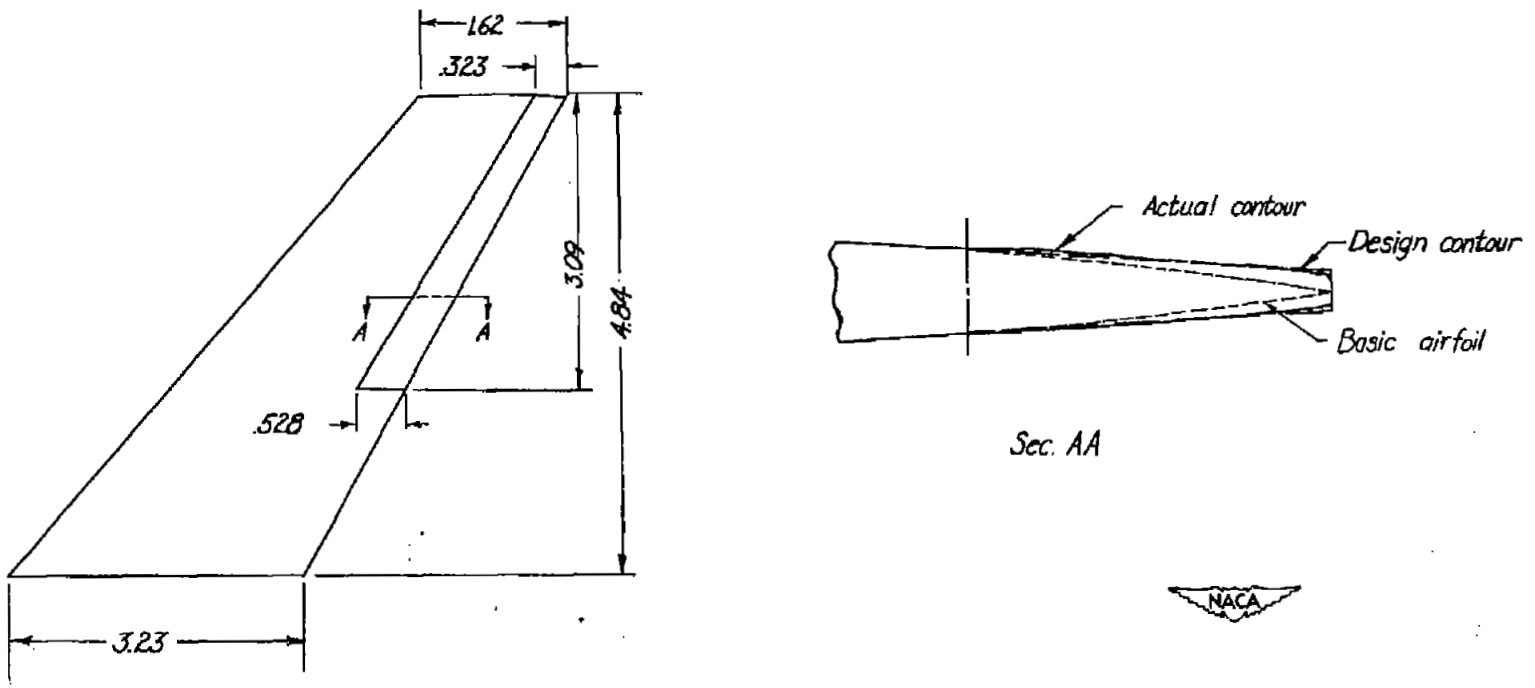

HALF-BLUNT AILERON

(b) Detail of half-blunt ailerons.

Figure 2.- Concluded.

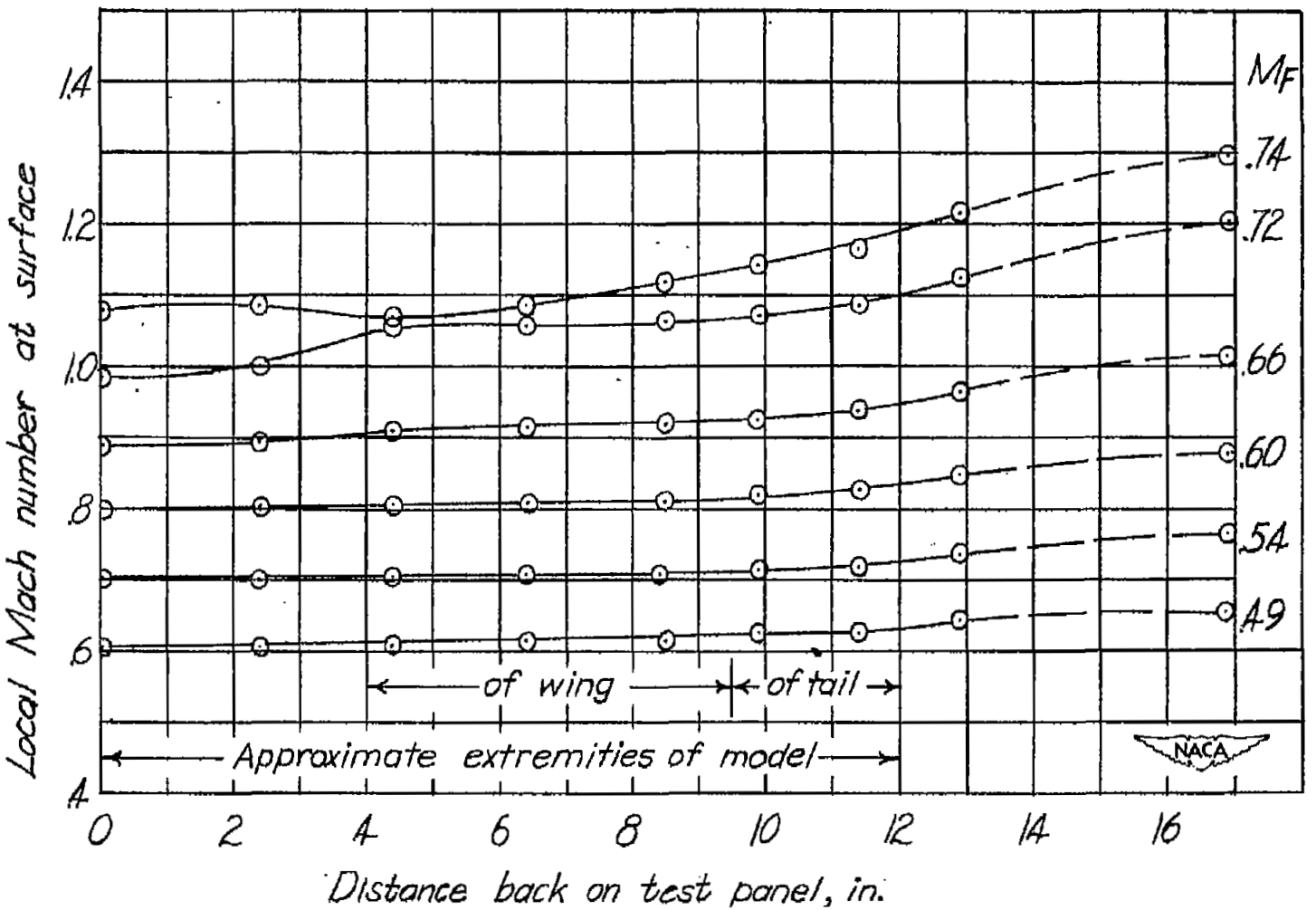

(a) Chordwise.

Figure 3.- Mach number gradients at the model location.

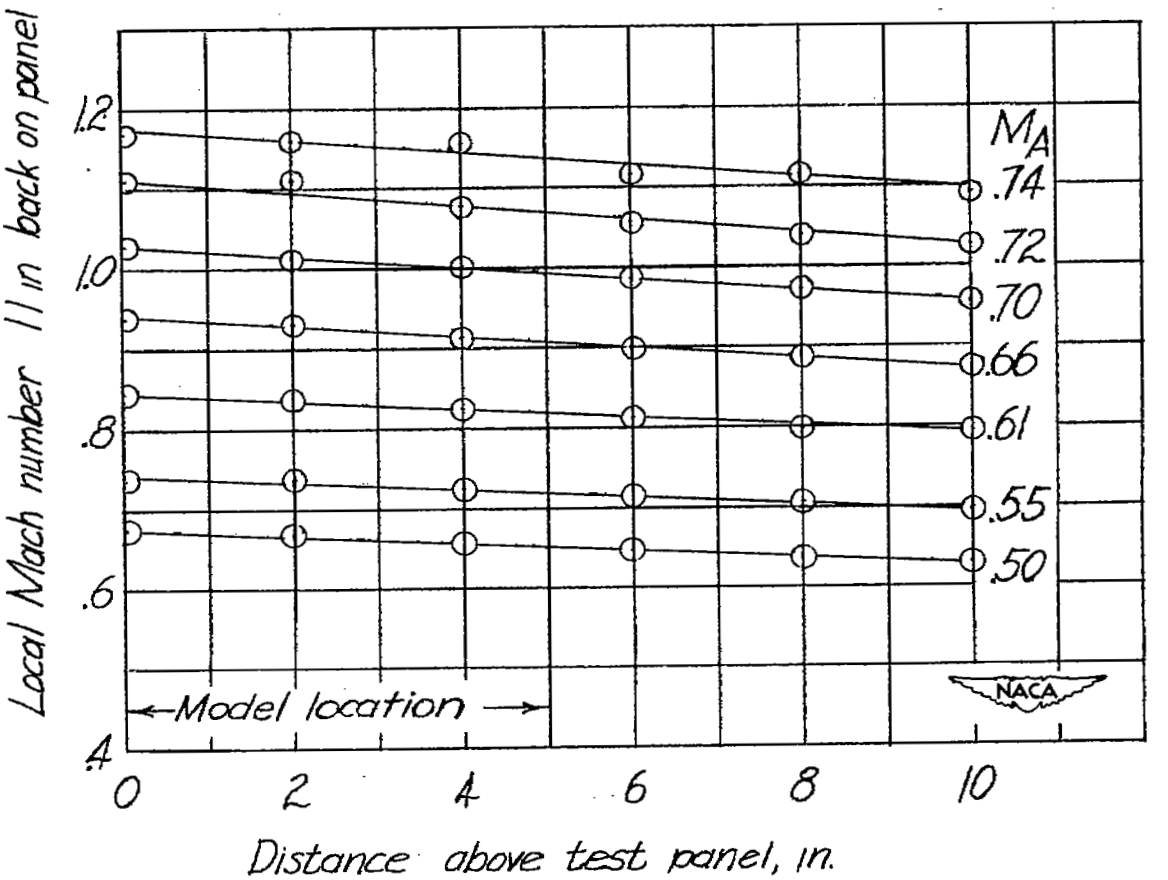

(b) Along the model span.

Figure 3.- Concluded.

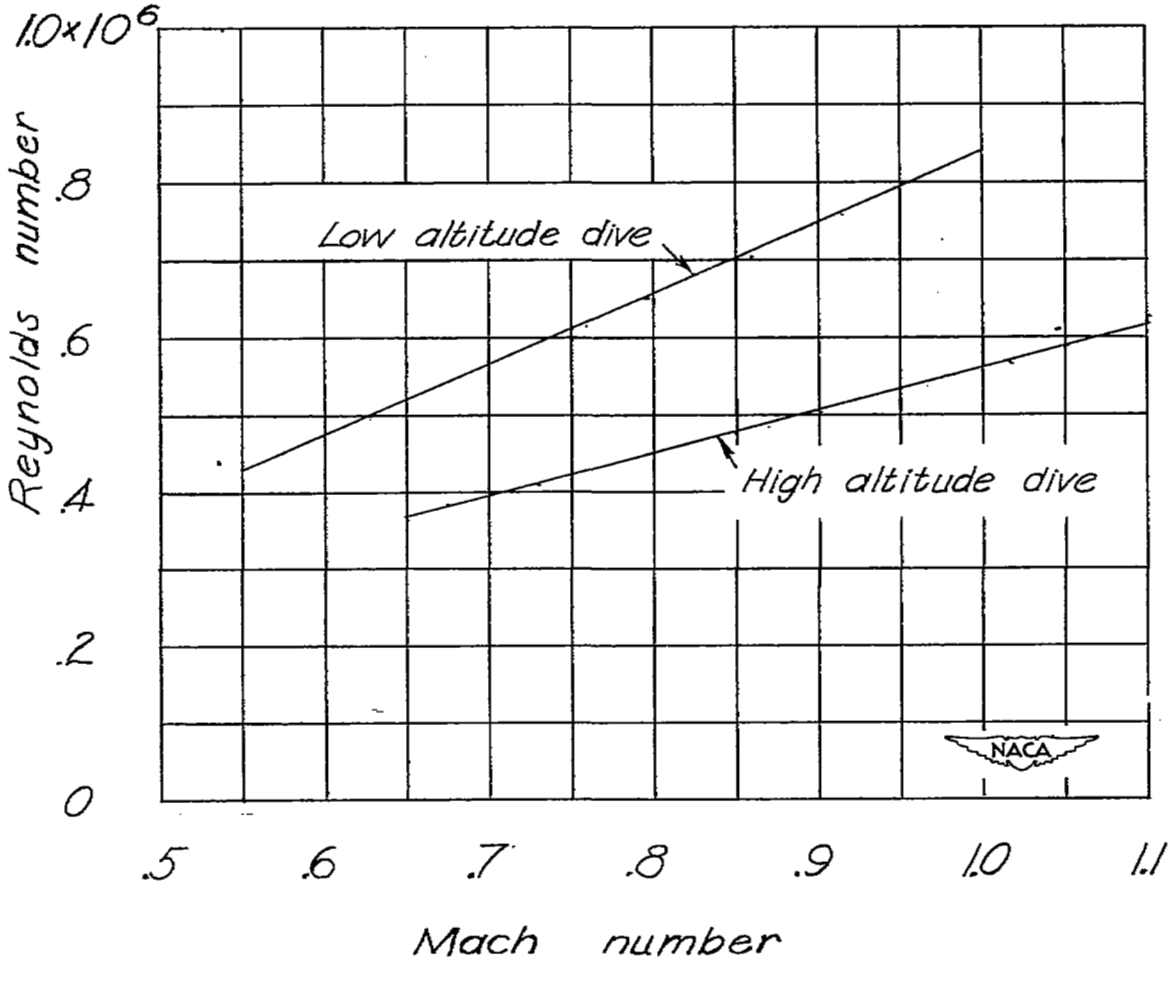

Figure 4.- Approximate variation of Reynolds number with Mach number based on the mean aerodynamic chord of wing.

[redacted]

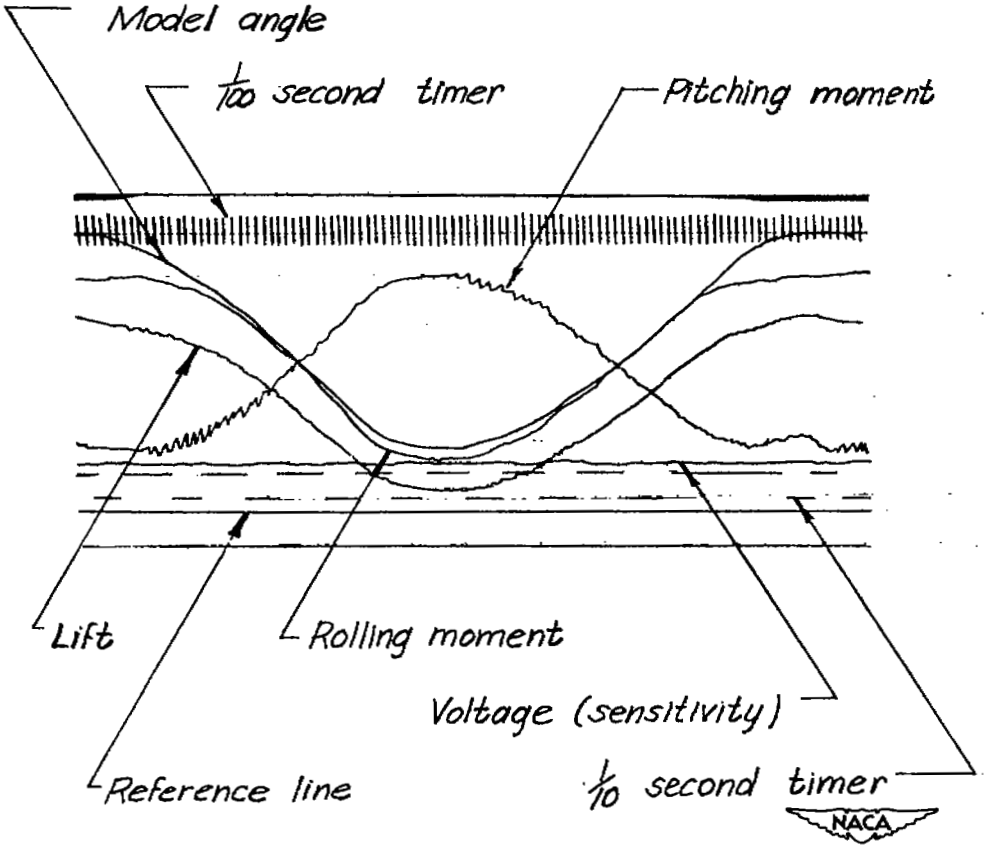

Figure 5.- Typical record from the recording galvanometer taken at M = 1.0 with tail set at 0° and model oscillating.

[redacted]

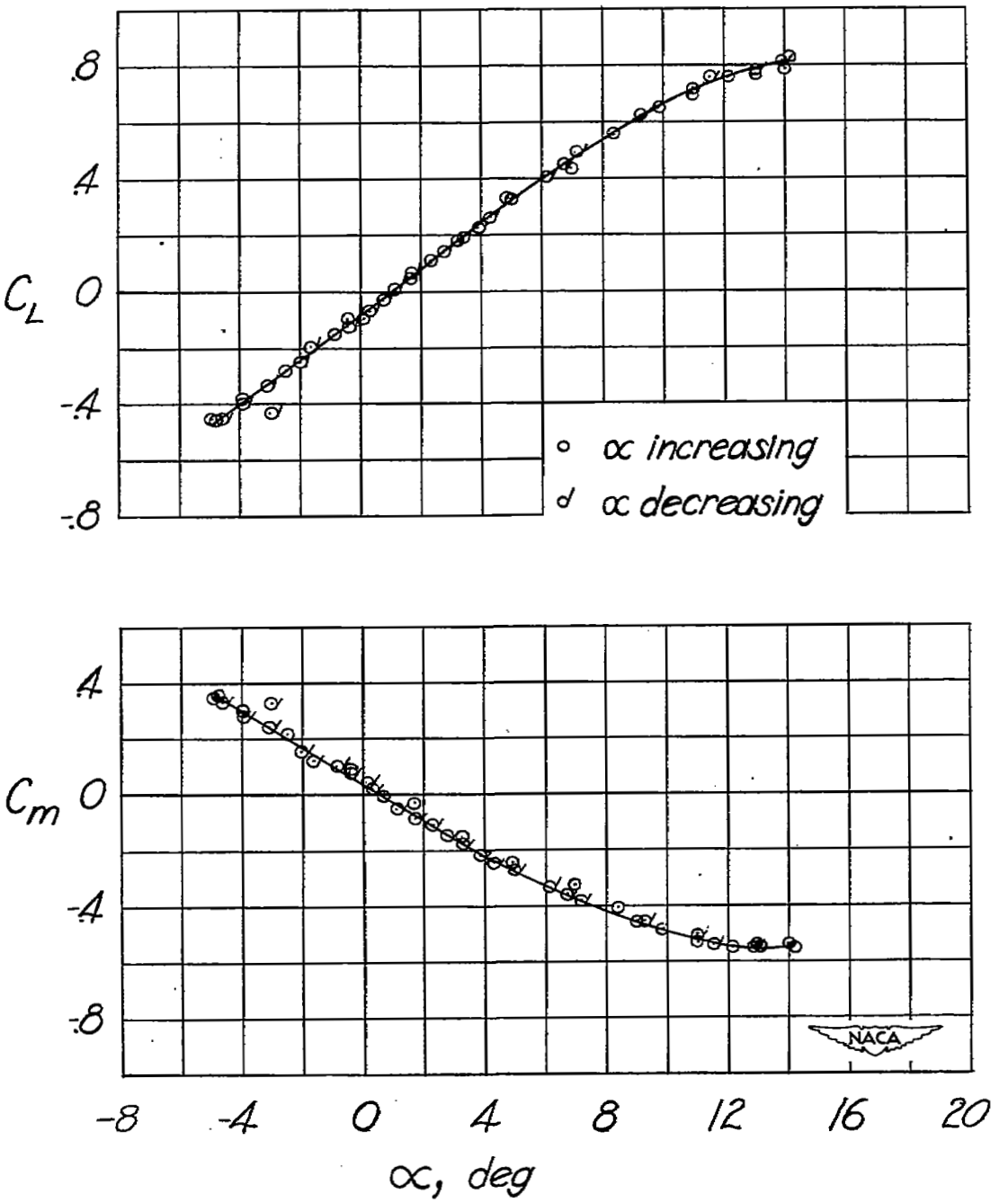

(a) Lift and pitching-moment characteristics; tail at 0°; M = 1.0; R = 560,000.

Figure 6.- Typical examples of wing-flow data.

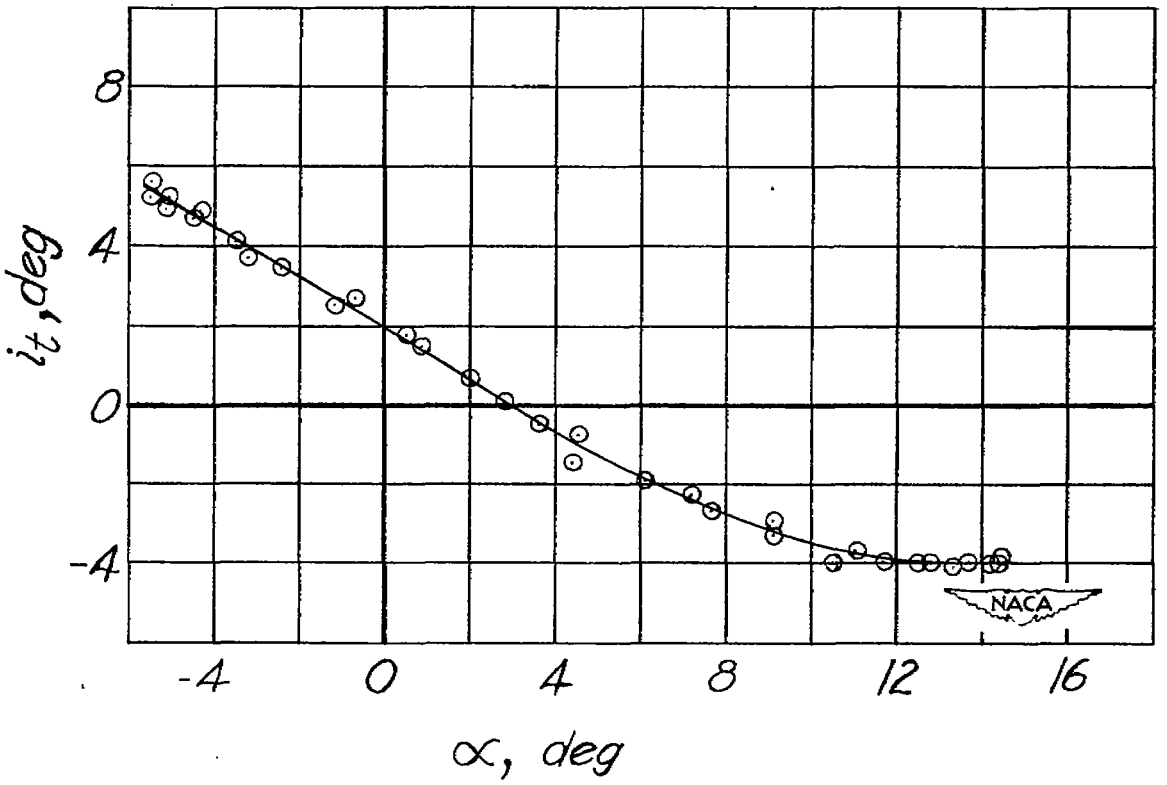

(b) Downwash test data obtained with model oscillating, tail floating free, M = 1.00; R = 560,000.

Figure 6.- Concluded.

[redacted]

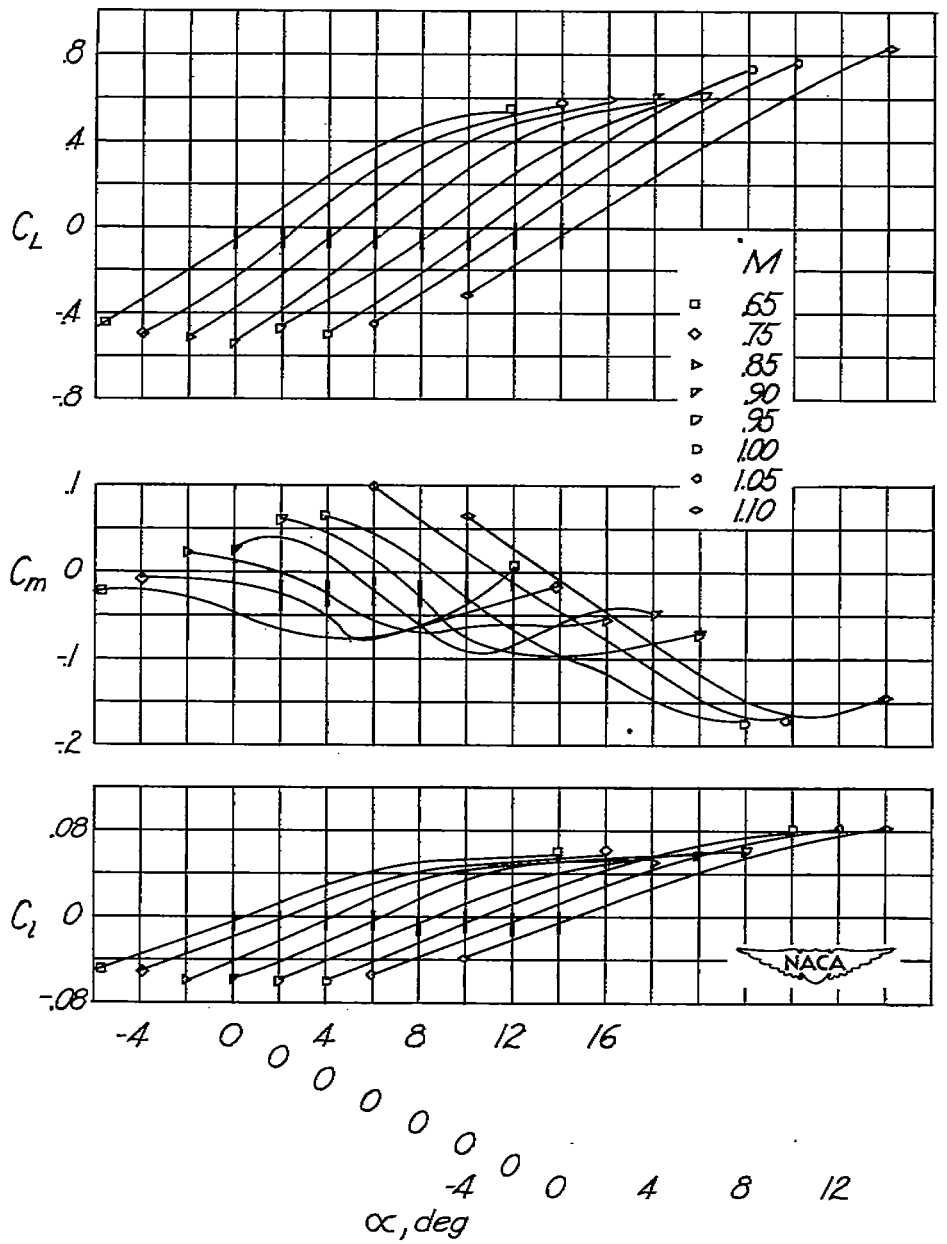

(a) Reynolds number from 360,000 to 620,000.

Figure 7.- Variation of the coefficients of lift, pitching moment about 23 percent $\bar{c}$, and rolling moment with angle of attack at Mach numbers throughout the test range for the model with tail removed. Note shift in abscissa zero for different Mach numbers. (Symbols do not represent test points.)

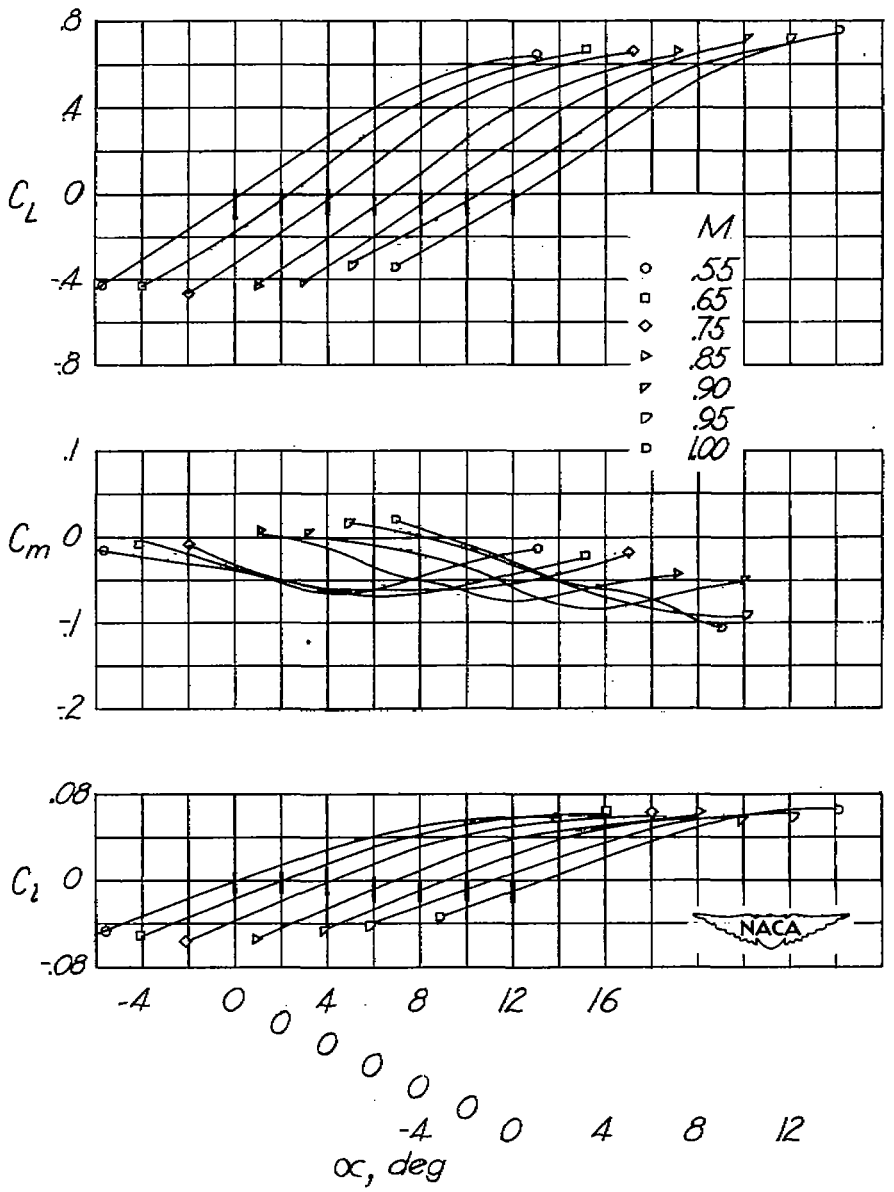

(b) Reynolds number from 430,000 to 840,000.

Figure 7.- Concluded.

[redacted]

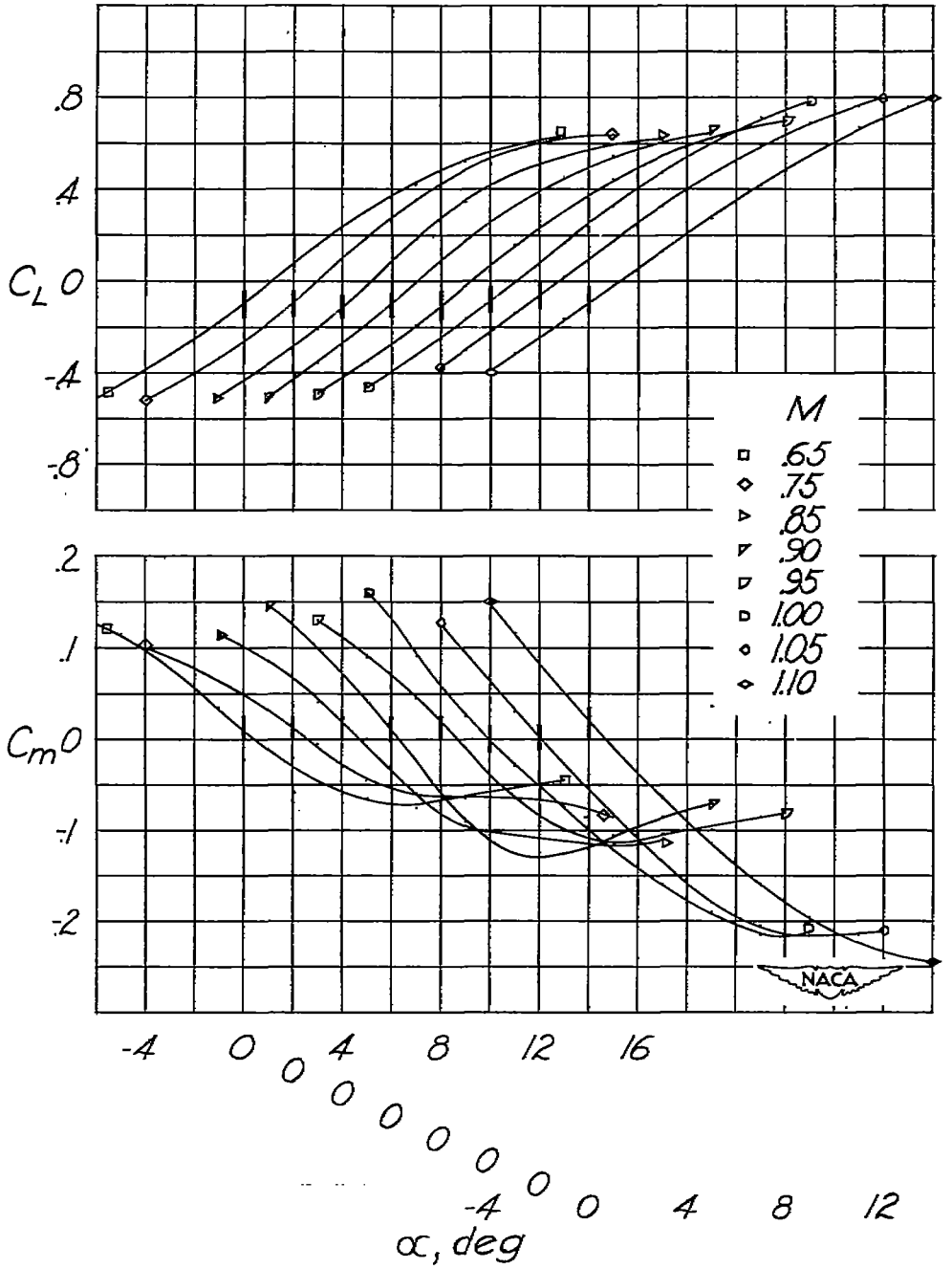

(a) Reynolds number from 360,000 to 620,000.

Figure 8.- Variation of coefficients of lift and pitching moment about 23 percent $\bar{c}$ at Mach numbers throughout the test range for the model with tail set at 0° with respect to wing chord line.

[redacted]

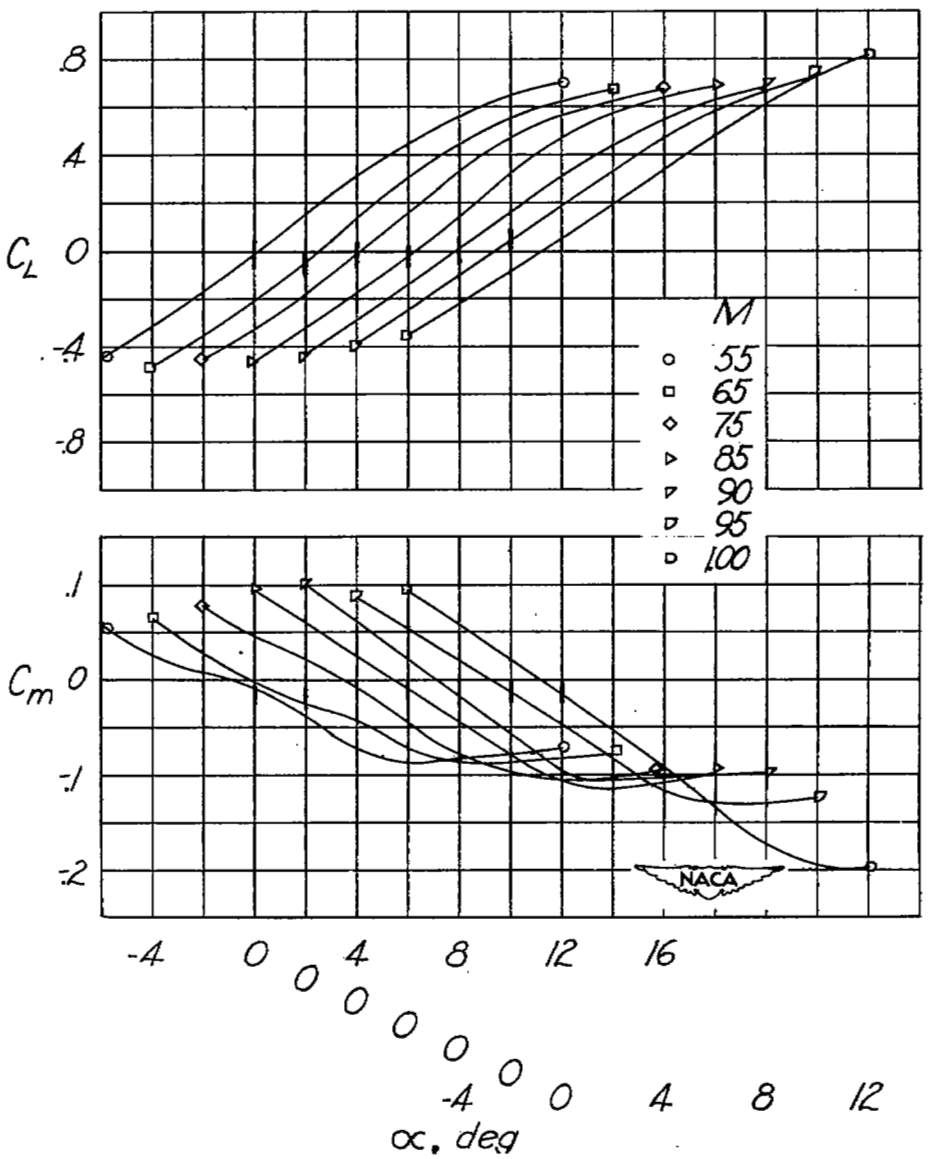

(b) Reynolds number from 430,000 to 840,000.

Figure 8.- Concluded.

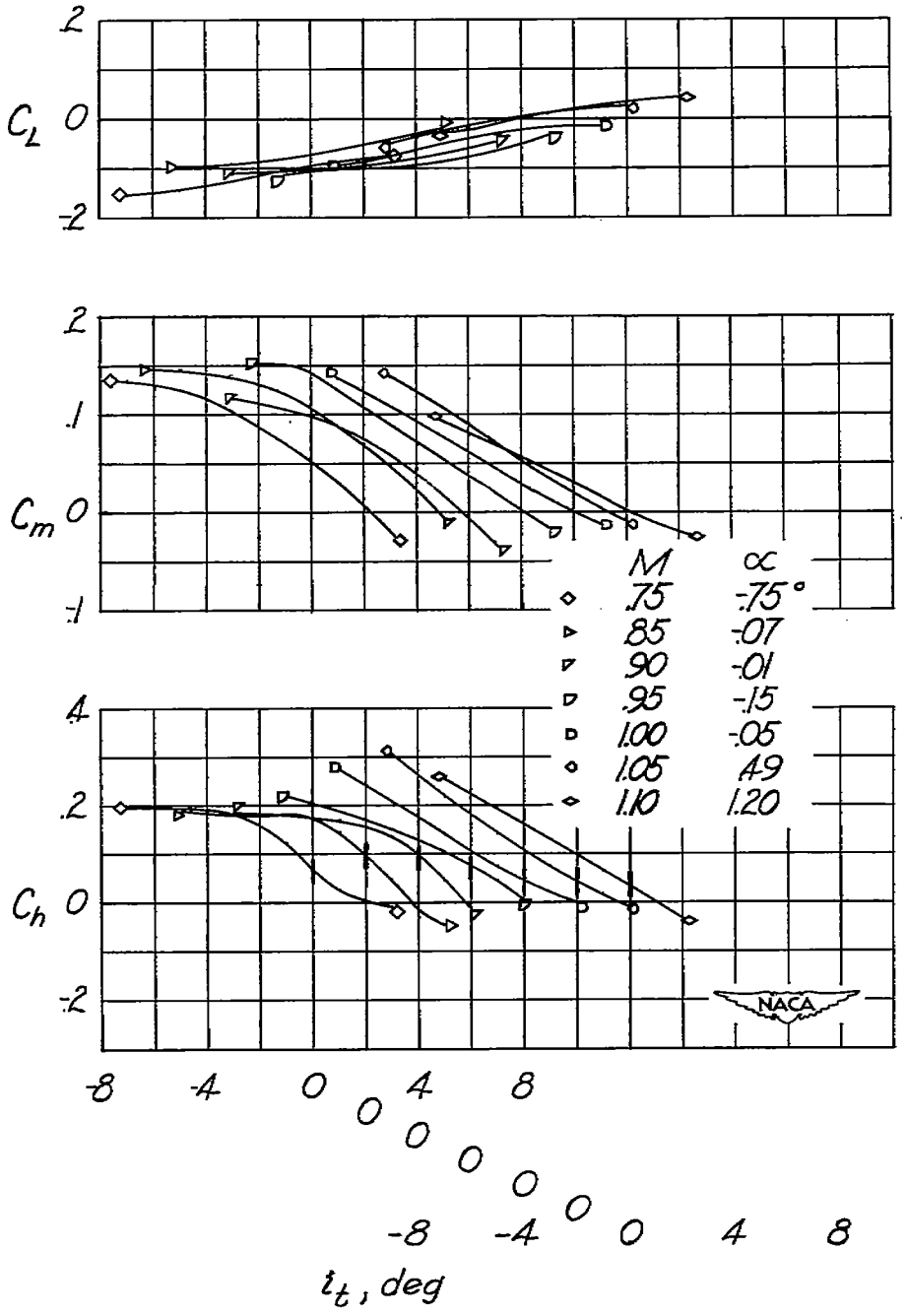

(a) Reynolds number from 420,000 to 620,000.

Figure 9.- Variations of the coefficients of lift, pitching moment about 23 percent $\bar{c}$, and hinge moment about -9.5 percent $\bar{c}_t$ with tail incidence at Mach numbers throughout the test range.

[redacted]

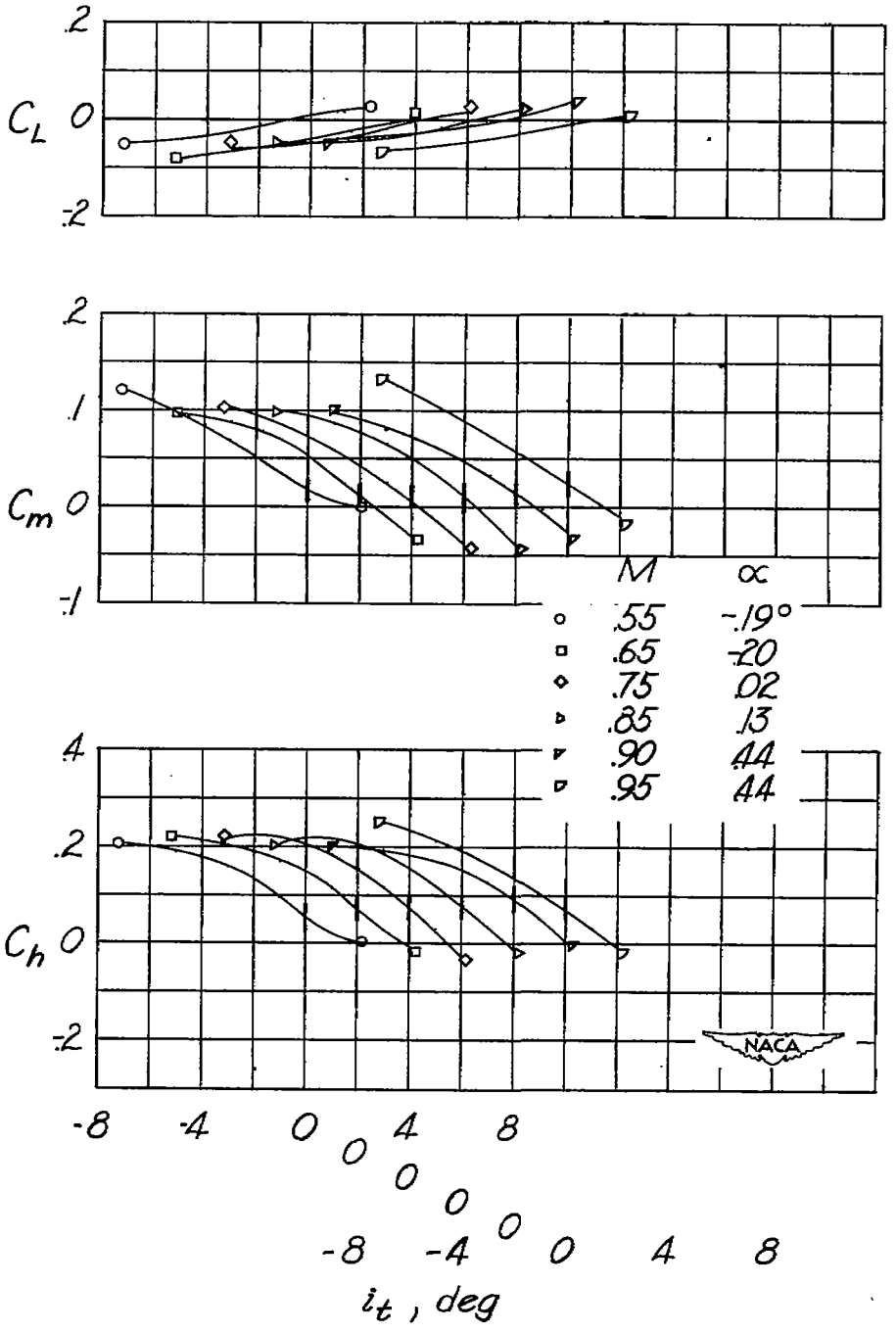

(b) Reynolds number from 430,000 to 800,000.

Figure 9.- Concluded.

[redacted]

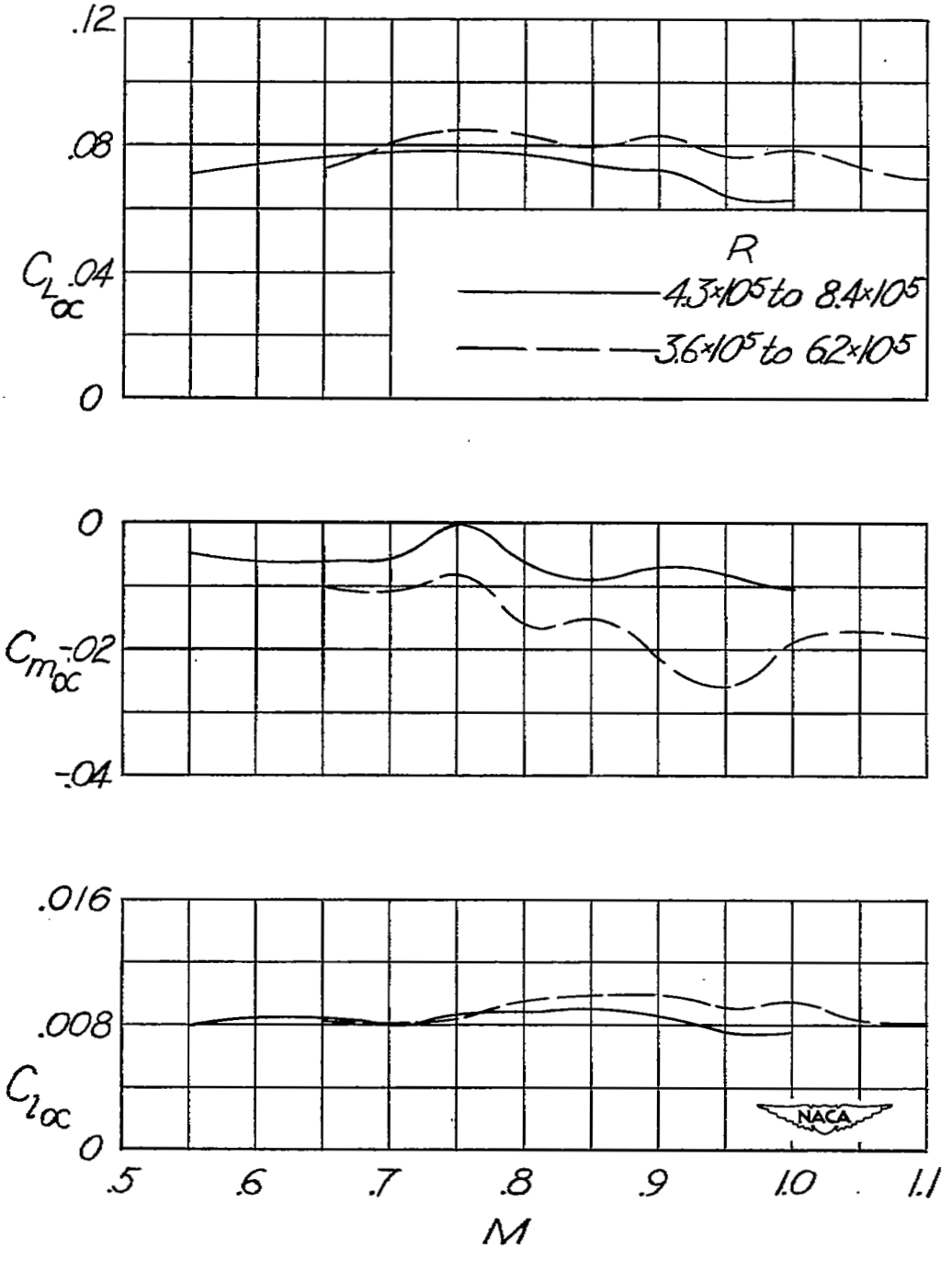

Figure 10.- Variation of C_{L_α}, C_{m_α}, and C_{l_α} at zero angle of attack with Mach number for two Reynolds number ranges for model with center of gravity at 23 percent $\bar{c}$, tail off.

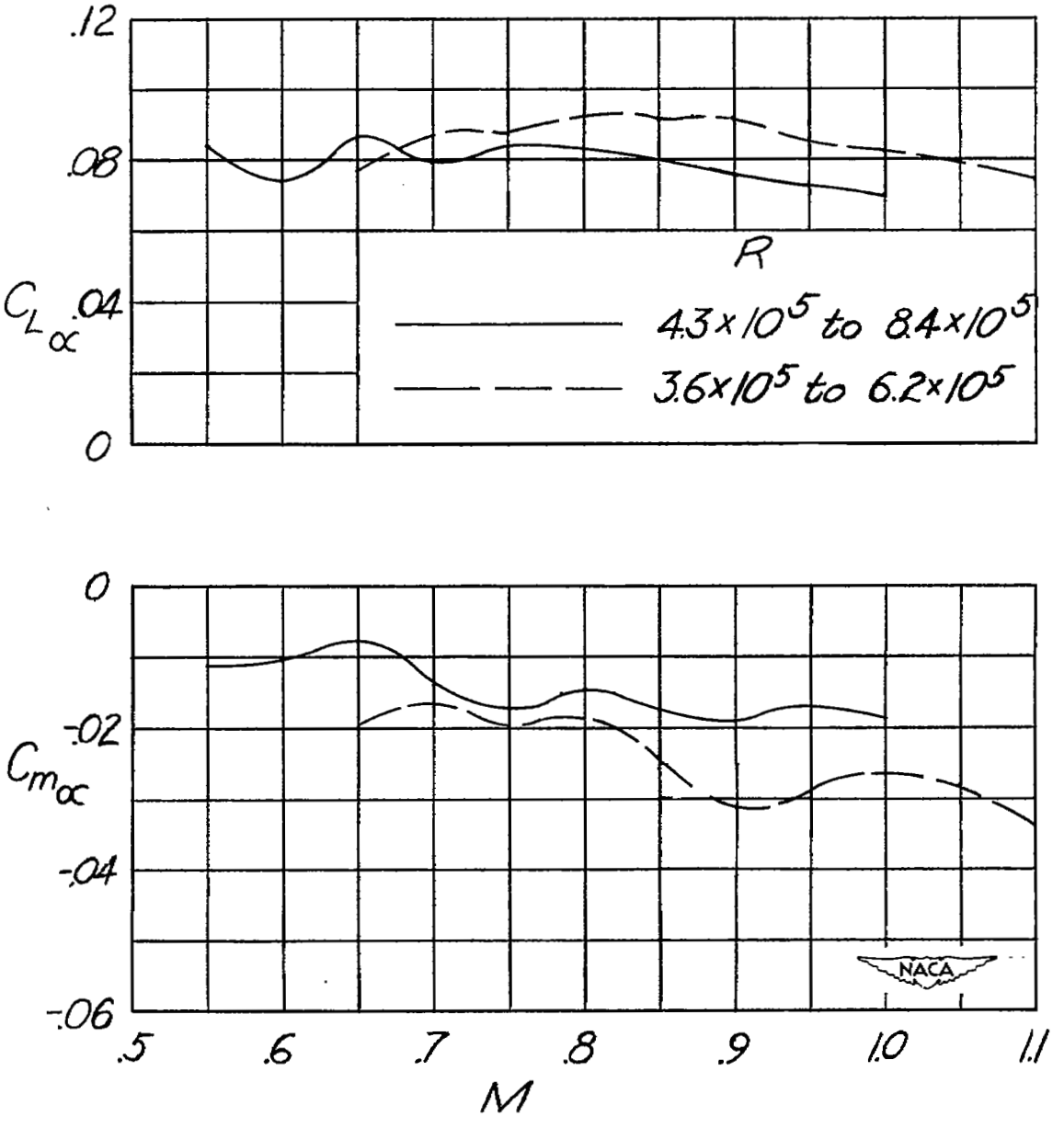

(a) C_{l_α} and C_{m_α}.

Figure 11.- Variation of longitudinal stability parameters measured at small angles of attack with Mach number for two Reynolds number ranges. Center of gravity at 23 percent $\bar{c}$ and $i_t = 0^\circ$ with respect to wing chordline.

[redacted]

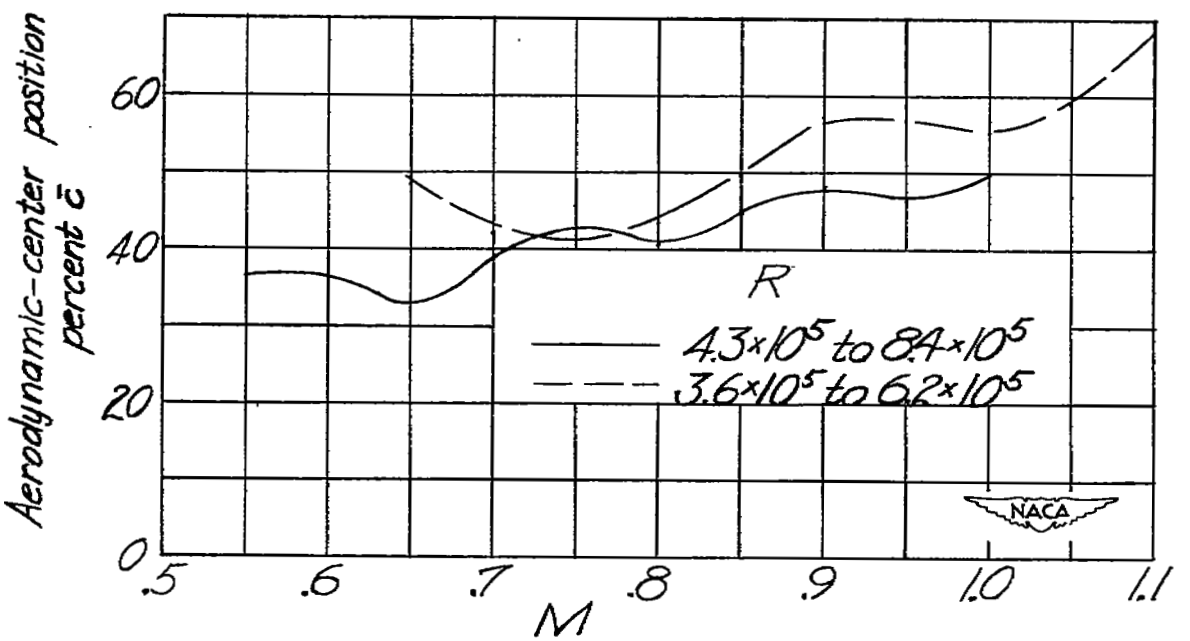

(b) $\frac{\partial C_m}{\partial C_L}$.

Figure 11.- Concluded.

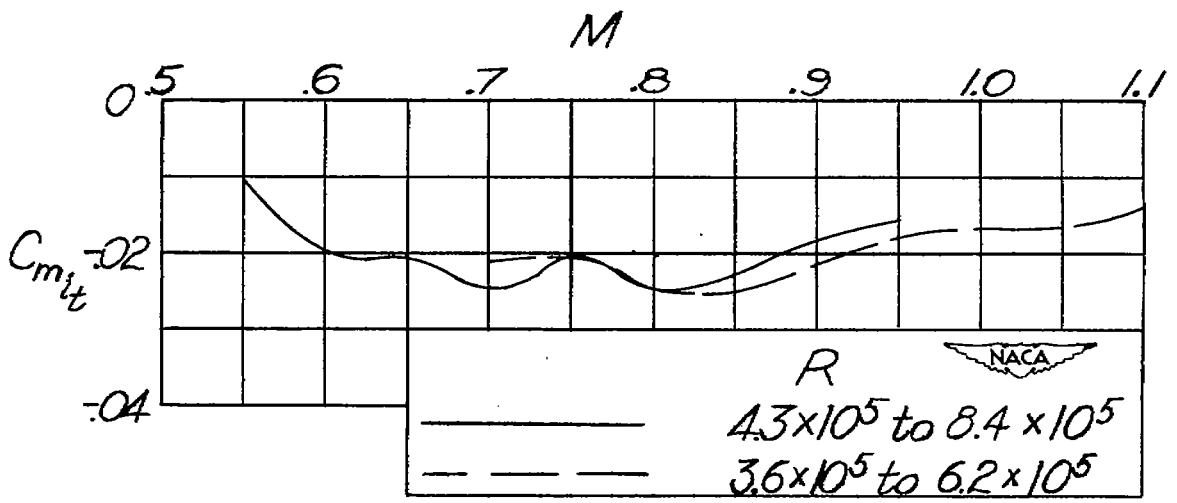

Figure 12.- Variation of $C_{m_{i_t}}$ about 23 percent $\bar{c}$ at zero angle of attack with Mach number for two Reynolds number ranges.

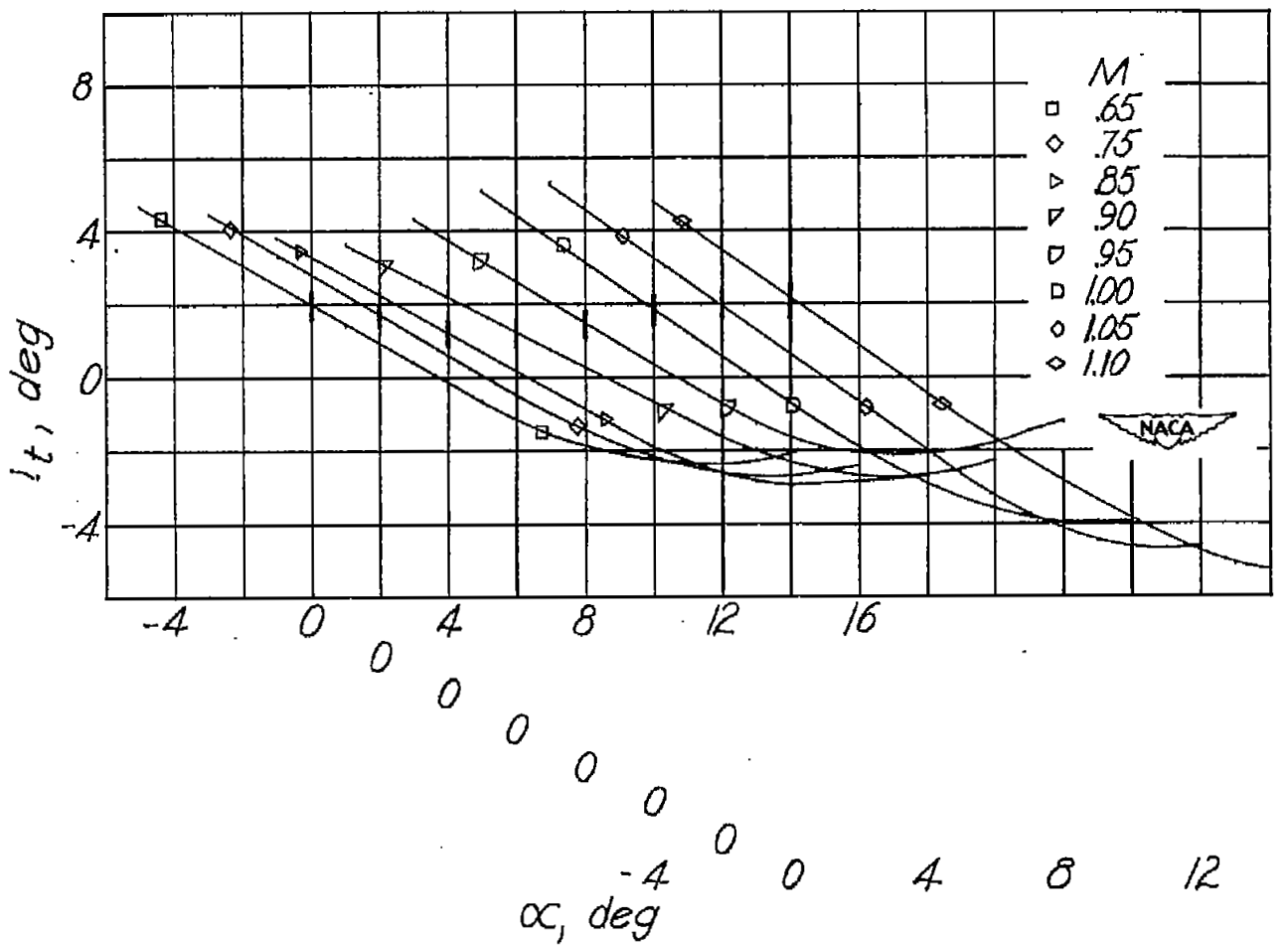

(a) Reynolds number from 360,000 to 620,000.

Figure 13.- Variation of free-floating tail angle with angle of attack for Mach numbers throughout the test range.

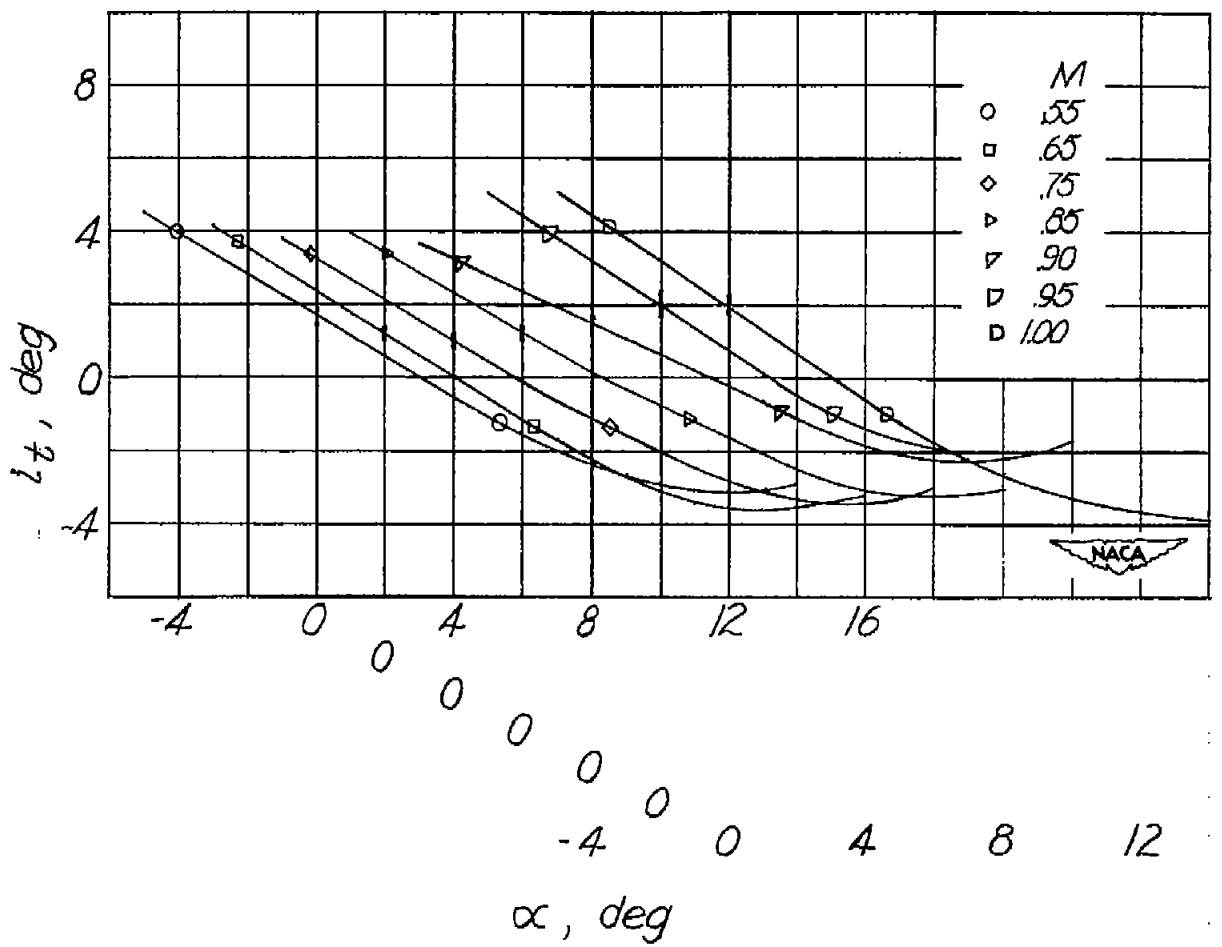

(b) Reynolds number from 430,000 to 840,000.

Figure 13.- Concluded.

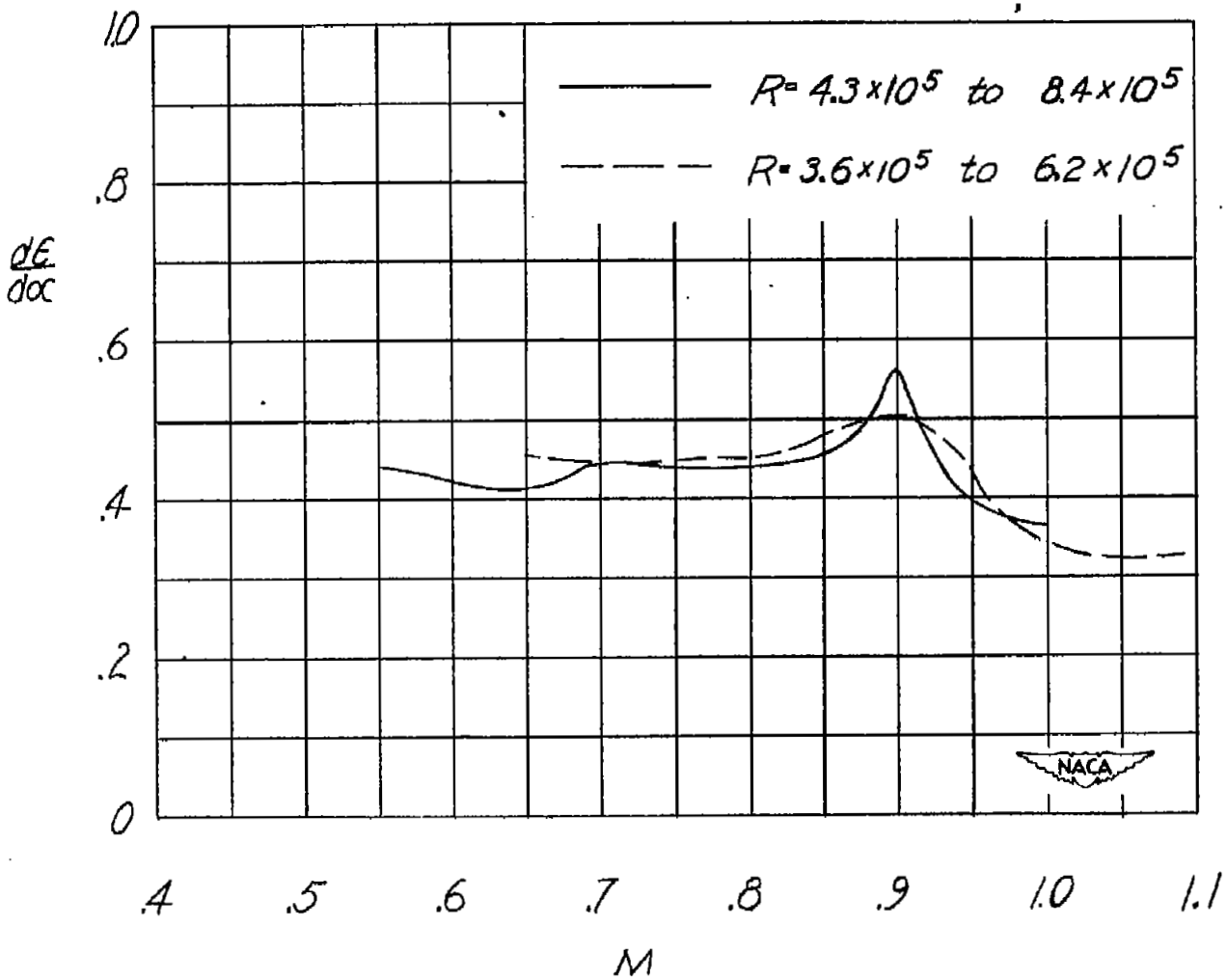

Figure 14.- Variation of downwash factor $\frac{d\epsilon}{d\alpha}$ at tail position with Mach number at low angles of attack.

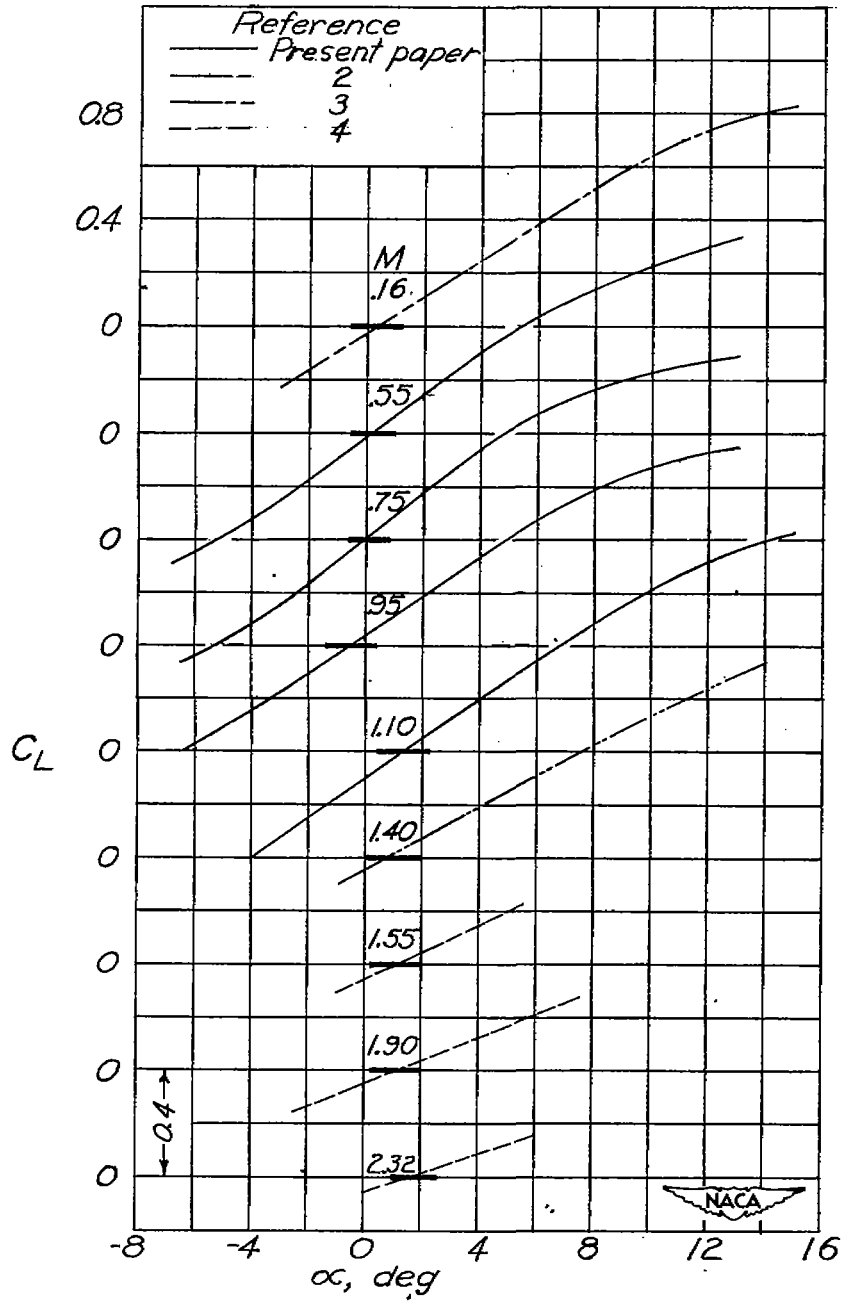

(a) Variation of lift coefficient with angle of attack.

Figure 15.- Combination of wing-flow data for the test configuration with tail on with data from other sources for lower and higher Mach numbers.

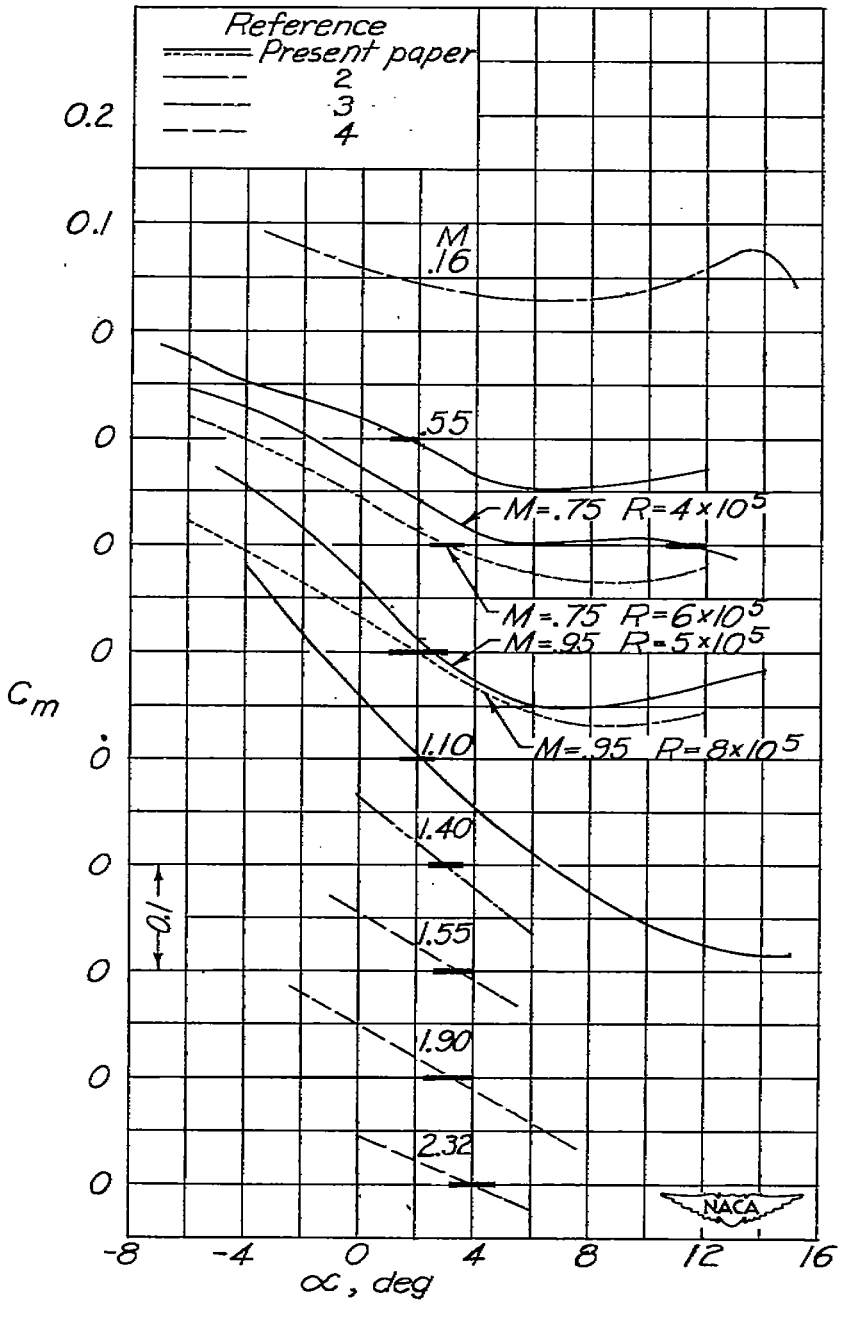

(b) Variation of pitching-moment coefficient with angle of attack for a stabilizer of incidence of -3° (angles measured with respect to wing chord line) with the center of gravity at 25 percent $\bar{c}$.

Figure 15.- Concluded.

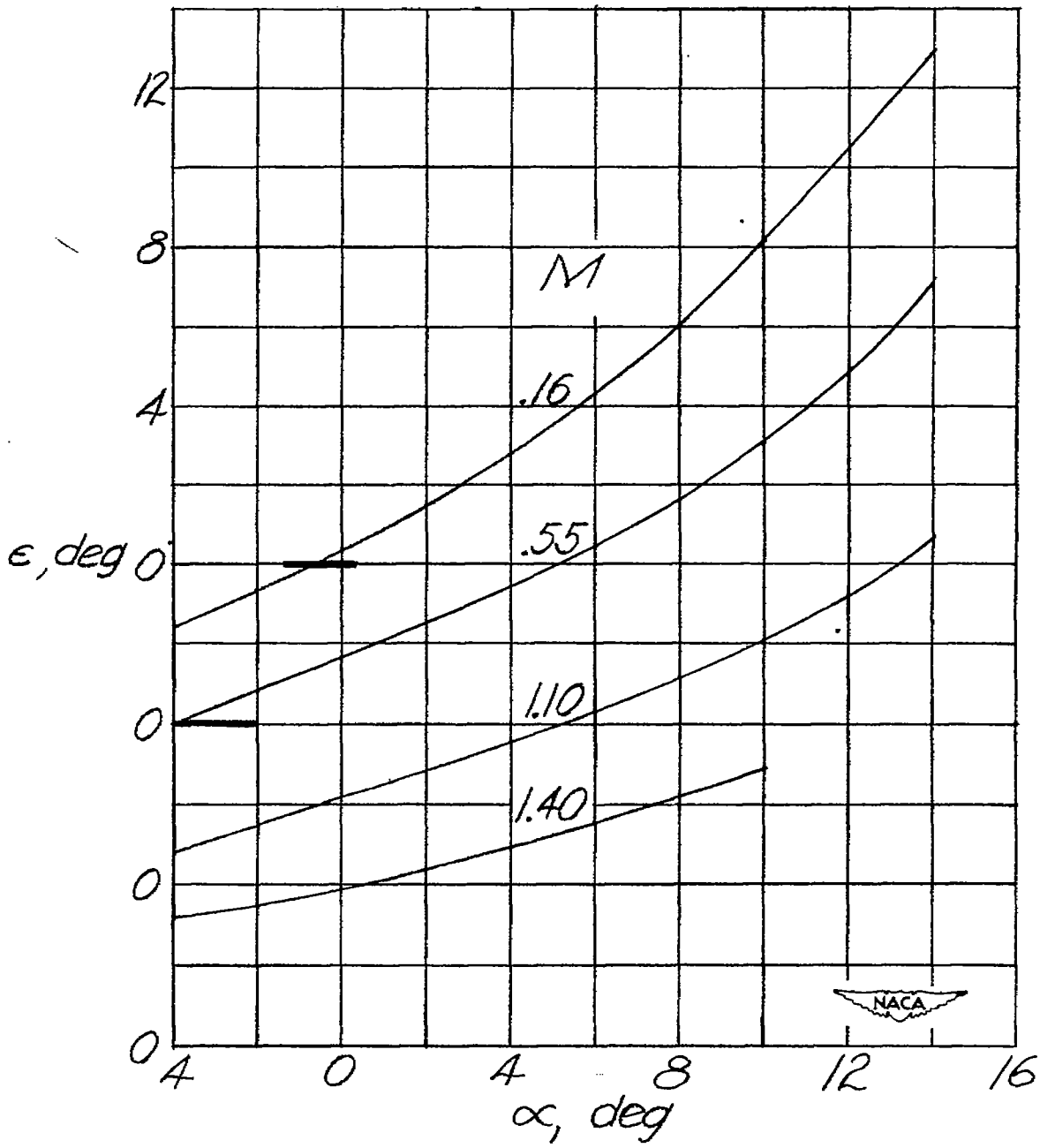

Figure 16.- Combination of wing-flow data with data from other sources for the test configuration showing the variation of downwash with angle of attack for a wide range of Mach numbers.

[redacted]